Journal of Alloys and Compounds 509 (2011) 3013–3018

Contents lists available at ScienceDirect

Journal of Alloys and Compounds

journal homepage: www.elsevier.com/locate/jallcom

Influence of the C14 $Ti_{35.4}V_{32.3}Fe_{32.3}$ Laves phase on the hydrogenation properties of the body-centered cubic compound $Ti_{24.5}V_{59.3}Fe_{16.2}$

A. Guéguen, J.-M. Joubert, M. Latroche*

Institut de Chimie et des Matériaux de Paris Est (ICMPE), Chimie Métallurgique des Terres Rares, CNRS, UMR 7182, Thiais, France

ARTICLE INFO

Article history:
Received 30 August 2010
Accepted 31 October 2010
Available online 3 December 2010

Keywords:
Multiphase alloys
Hydrogen storage materials
XRD
EPMA

ABSTRACT

Bcc $Ti_{24.5}V_{59.3}Fe_{16.2}$ alloys containing 10 and 30% of C14 Laves phase inclusions were prepared by induction melting followed by annealing at 1000 °C. X-ray powder diffraction and BSE microscopy confirmed the presence of the C14 Laves phase (average composition $Ti_{35.4}V_{32.3}Fe_{32.3}$) embedded in the bcc matrix. The two end members of the series, the C14 Laves phase and the bcc $Ti_{24.5}V_{59.3}Fe_{16.2}$ alloy, have very different hydrogenation behaviors. The C14 Laves phase does not absorb as much hydrogen as does the bcc phase. No equilibrium plateau and little hysteresis between absorption and desorption were observed at 25 °C for the C14 Laves on the PCI curves whereas those of the bcc sample present one equilibrium plateau and significant hysteresis between absorption and desorption. As a result, the absorption capacity and the length of the equilibrium plateau of the multiphase alloys decrease with the C14 Laves phase content. The hydrogenation properties of an as-cast bcc $Ti_{24.5}V_{59.3}Fe_{16.2}$ sample were also investigated: the kinetics of the first hydrogenation is found to be slower and the plateau pressures higher for the as-cast alloy than for the annealed sample.

© 2010 Elsevier B.V. All rights reserved.

1. Introduction

Several families of metallic hydrides are studied for hydrogen storage application: AB_5, AB_2 and AB type materials, where A is an element with high affinity for hydrogen such as rare earth elements and B an element with low affinity for hydrogen (typically a transition metal). The hydrogen sorption properties of vanadium metal, because of its low atomic mass, have also been extensively studied [1,2]. Hydrogenation of vanadium occurs by the successive formation of two hydrides; it can take reversibly up to 2.2 wt%. However vanadium presents several disadvantages: first, it is an expensive element, then part of the hydrogen absorbed can not be recovered because of the stability of the monohydride. Finally thermal treatments are needed to activate the metal.

A way to reduce the cost of such storage material and to improve the reactivity of vanadium is to alloy it with other elements. Ono and co-workers considered Ti–V alloys [3]. The two elements form a bcc solid solution which reacts with hydrogen without any pretreatment. However the kinetics are still slow. Maeland et al. observed that, when a small amount of atoms which radius is smaller than 95% of the initial element (Fe, Cr, Mn or Ni in the case of vanadium) was added to $Ti_{0.70}V_{0.30}$, no treatment was necessary to start the reaction at room temperature and its rate was much faster [4]. Ti–V–Cr alloys can absorb hydrogen reversibly up to 2.4 wt [5–9]. Chromium is still an expensive element; the use of a cheaper transition metal instead of chromium would be economically more viable. Work by Challet [10] on the bcc alloys $(Ti_{0.355}V_{0.645})_{100-x}M_x$ (M = Mn, Fe, Co, Ni, x = 7, 14 and 21) demonstrated that the best results for hydrogen storage were obtained for Fe.

Secondary phase precipitation has been used to improve the reaction kinetics and electrochemical activity of several intermetallic hydride [11–14]. For example, Joubert et al. observed significant enhancement of the discharge capacities of multiphase alloys in the Zr–Ni–Cr system [11]. Such materials were prepared by precipitation of secondary Zr–Ni phases in a Laves phase matrix. La also does not dissolve into the Laves phase $Zr(Cr_{0.4}Ni_{0.6})_2$ but combine with Ni to form LaNi precipitates. The multiphase alloy showed better activation than $Zr(Cr_{0.4}Ni_{0.6})_2$ [14]. Improved kinetics were also reported by Bououdina et al. in multiphase alloys prepared from Laves phase and $LaNi_5$ [12]. $V_3TiNi_{0.56}Hf_{0.24}$ is composed of a bcc Ti–V based solid solution and a $MgZn_2$-type Laves phase structure forming a 3D network in the alloy [15]. The bcc solid solution is mainly responsible for hydrogen storage while the C14 phase helps the formation of cracks in the alloy, thus increasing the rate of the reaction. Akiba et al. developed the concept of hydrogen absorption by Laves phase related bcc solid solution [13]. Several AB_2-type alloys do not form pure solid solution but always crystallise with bcc solid solution phases ($Zr_{0.5}Ti_{0.5}MnV$ for example [16]). The composition TiMnV cannot be prepared as a single solid

* Corresponding author. Tel.: +33 1 49 78 12 10; fax: +33 1 49 78 12 03.
E-mail addresses: michel.latroche@icmpe.cnrs.fr, latroche@glvt-cnrs.fr (M. Latroche).

0925-8388/$ – see front matter © 2010 Elsevier B.V. All rights reserved.
doi:10.1016/j.jallcom.2010.10.213

Table 1
Nominal composition of the different alloys studied, their expected *C*14 Laves phase content, type of the different phases present in each sample, their chemical composition obtained from EPMA analysis and their *C*14 Laves phase content and cell parameters obtained from powder XRD refinements.

Sample No.	Nominal composition	Expected content of *C*14 Laves phase (%)	Type of phase	Composition	Refined wt% content the phase	Cell parameters (Å)
1	$Ti_{24.5}V_{59.3}Fe_{16.2}$	0	bcc	$Ti_{25.2(7)}V_{59.5(9)}Fe_{15.3(3)}$	96.2 (5)	a = 3.0357 (4)
			*C*14	$Ti_{35.1(13)}V_{33.4(12)}Fe_{31.6(15)}$	3.8 (5)	a = 4.908 (4)
						c = 8.041 (1)
1′	$Ti_{24.5}V_{59.3}Fe_{16.2}$	0	bcc	$Ti_{25.1(25)}V_{59.1(39)}Fe_{15.8(14)}$	100	a = 3.0427 (4)
2	$Ti_{25.6}V_{56.6}Fe_{17.8}$	10	bcc	$Ti_{27.4(3)}V_{55.9(3)}Fe_{16.7(1)}$	90.4 (7)	a = 3.0418 (6)
			*C*14	$Ti_{35.8(2)}V_{32.1(2)}Fe_{32.1(1)}$	9.6 (7)	a = 4.912 (2)
						c = 8.048 (6)
3	$Ti_{27.45}V_{51.5}Fe_{21.05}$	30	bcc	$Ti_{26.7(1)}V_{56.1(2)}Fe_{17.3(1)}$	75.3 (1)	a = 3.0374 (6)
			*C*14	$Ti_{34.9(2)}V_{32.6(3)}Fe_{32.4(1)}$	24.7 (1)	a = 4.91213 (7)
						c = 8.0046 (2)
4	$Ti_{35}V_{30}Fe_{35}$	100	*C*14	$Ti_{34.6(2)}V_{30.8(2)}Fe_{34.7(3)}$	100	a = 4.9125 (5)
						c = 8.0054 (7)

Note: The samples 1, 2, 3 and 4 were annealed at 1000 °C for 2 weeks after fusion, 1′ was studied as cast.

solution, *C*14 phases are always observed inside the bcc matrix. TEM analysis of the bcc/*C*14 interface indicates the presence of fine lamellar structure (width ∼200 nm). The capacity of an alloy with the composition identical to this interface neighbor was found to be 1.5–2 times larger than that of the original matrix alloy [17].

Fe has a limited solubility in Ti–V alloys. Based on the work of Tsin Khua and Kornilov on Fe_2Ti–V, Fe–Ti and Ti–V–Fe systems [18,19], Raghavan, Cornish and Watson proposed an isothermal section at 1000 °C of the ternary system [20,21]. However results obtained by Challet on the $(Ti_{0.355}V_{0.645})_{100-x}Fe_x$ alloys disagree with the solubility limit of Fe in the Ti–V rich bcc solid solution [10]. Massicot et al. reinvestigated the isothermal section at 1000 °C of the Ti–V–Fe system and proposed a new phase diagram [22]. They did not find other phase than those reported for the binary systems, namely the bcc, *B*2 and the *C*14 Laves phases (Fig. 1). The *C*14 Laves phase was shown to be in equilibrium with the bcc phase in a very large composition domain. The hydrogenation properties of several bcc alloys were also studied by Massicot et al. since the Ti/V/Fe ratios allows a fine tuning of the equilibrium pressure [23]. They could relate the formation and dissociation enthalpy of a bcc alloy to the molar fraction of Ti, V and Fe. Knowing the boundaries of both the *C*14 and bcc phase domain, we decided to investigate the effect of *C*14 phase precipitation on the hydrogen sorption properties of the bcc phase. Materials containing 10 and 30% of *C*14 Laves phases embedded in a matrix of composition $Ti_{24.5}V_{59.3}Fe_{16.2}$ were prepared by induction melting and annealed at 1000 °C. The homogeneity and the chemical composition of the samples were studied using powder X-ray diffraction (XRD) and electron probe micro-analysis (EPMA). Hydrogen sorption properties were also investigated. The structural information and hydrogen absorption properties of these materials will be compared with those collected by Massicot on the *C*14 laves phase compound $Ti_{35}V_{30}Fe_{35}$ [24]. In order to estimate the influence of the annealing step on the structure of the samples, the pure bcc sample $Ti_{24.5}V_{59.3}Fe_{16.2}$ was also prepared without annealing.

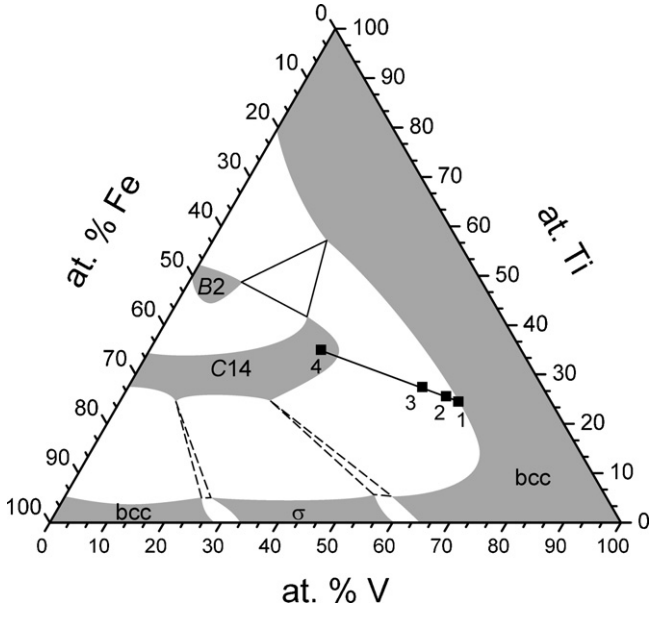

Fig. 1. Isothermal section of the Fe–Ti–V phase diagram at 1000 °C. The 4 compounds considered (■) lie along the tie-line joining the *C*14 and bcc phase domains.

2. Experimental

All samples were synthesized by melting high purity elements (Ti 99.99% from Alfa Aesar, V 99.9% from ChemPur and Fe 99.98% from Sigma-Aldrich) in an induction furnace in a water-cooled copper hearth furnace under argon atmosphere. The ingots were melted five times and turned over each time to ensure a good homogeneity of the samples. After fusion, the ingots were wrapped in a tantalum foil, annealed in silica tubes at 1000 °C for 2 weeks under Ar atmosphere and quenched in water to remove any concentration gradient created during cooling and to put the samples in a state close to equilibrium.

X-ray powder diffraction was collected at room temperature on a Bruker D8 Advance (Cu Kα, Bragg Brentano geometry, 2θ range 20–120°, step size 0.02°). As the materials were hard and ductile, a fine powder could not be obtained by grinding. The samples were prepared by filing the ingots. All the patterns were refined with the Rietveld method using the program TOPAS [25].

The chemical analysis was performed on finely polished samples using an EPMA Cameca SX 100. The repartition of the second phase in the bcc matrix was studied using Backscattered Electron Microscopy (BSE). Accelerating voltage and beam current were 15 kV and 40 nA respectively. The composition of each phase in the alloys was determined from 10 to 100 measurements.

The pressure–composition–isotherm (PCI) curves were measured with a Sieverts type apparatus. As the compounds were hard to break, no powder could be used for the experiment. Coarse grains were obtained by breaking the ingot with a hammer and an Abiche mortar. All manipulations before exposure to pure hydrogen gas (99.9999% from Alphagaz) were carried out in air. Activations were performed at 25 °C under 25 bar of hydrogen. A thermal treatment was necessary to fully desorb the sample: the sample holder was heated over one hour up to 500 °C under primary vacuum containing residual hydrogen gas and then cooled down to room temperature. The cycle was repeated four times to ensure complete reaction of the material with hydrogen before collection of the PCI curves. Absorption kinetics studies were also performed during the last activation cycle.

3. Results and discussion

3.1. Structural characterizations

Four samples (1–4) were synthesized, the composition of which are chosen along one tie-line joining the *C*14 and the bcc domains in the ternary section at 1000 °C [22]. They should, in principle, consist

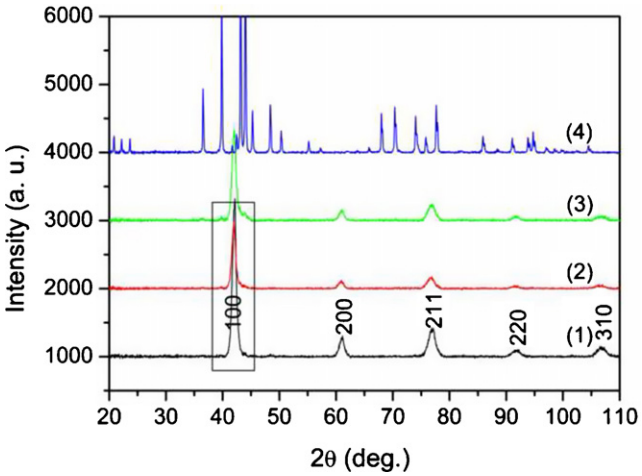

Fig. 2. Powder X-ray diffraction patterns of alloys 1, 2, 3 and 4.

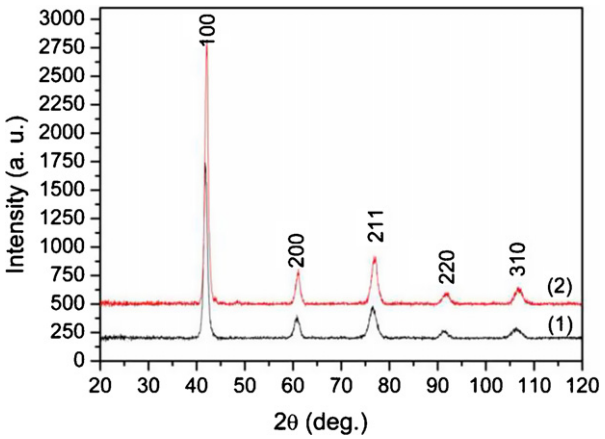

Fig. 3. Powder X-ray diffraction patterns of $Ti_{24.5}V_{59.3}Fe_{16.2}$ (1) annealed (alloy 1) and (2) as-cast (alloy 1′).

in the same two phases with the same compositions but variable amounts (Fig. 1, Table 1).

The powder XRD patterns for compounds 1, 2, 3 and 4 are shown in Fig. 2. The most intense peaks could be indexed as the bcc phase. However minor peaks of low intensity in the region 35–45° are observed for all compounds. The intensity of these peaks increases with the amount of second phase content. They are hardly visible in the case of $Ti_{24.5}V_{59.3}Fe_{16.2}$, only a light shoulder is noticeable. The position of these peaks indicates a hexagonal *C*14 Laves phase. Rietveld analysis was performed using the program TOPAS. The lattice parameters and the weight fraction of both phases in each material can be found in Table 1.

The XRD diffraction powder patterns were collected for the as-cast and annealed $Ti_{24.5}V_{59.3}Fe_{16.2}$ samples (Fig. 3). The patterns are similar, both indicate a bcc phase. The as-cast sample seems to be single-phase as no shoulder can be observed around the main peak at 42°.

In order to confirm these results, BSE microscopy and EPMA analysis were performed on finely polished samples for all compositions. *C*14 Laves phase inclusions appear as brighter areas on BSE images for compounds 1, 2 and 3. The study confirms the presence of a small amount of *C*14 Laves phase embedded in the bcc matrix in the case of $Ti_{24.5}V_{59.3}Fe_{16.2}$ (Fig. 4a). As the second phase content increases, a higher amount of inclusions was observed for compounds Nos. 2 and 3 which nominally contain 10 and 30% of second phase (Fig. 4b). In the case of as-cast $Ti_{24.5}V_{59.3}Fe_{16.2}$, no second phase was observed in the bcc matrix (Fig. 4c). The composition $Ti_{24.5}V_{59.3}Fe_{16.2}$ is close to the limit of the bcc domain, this may result in the

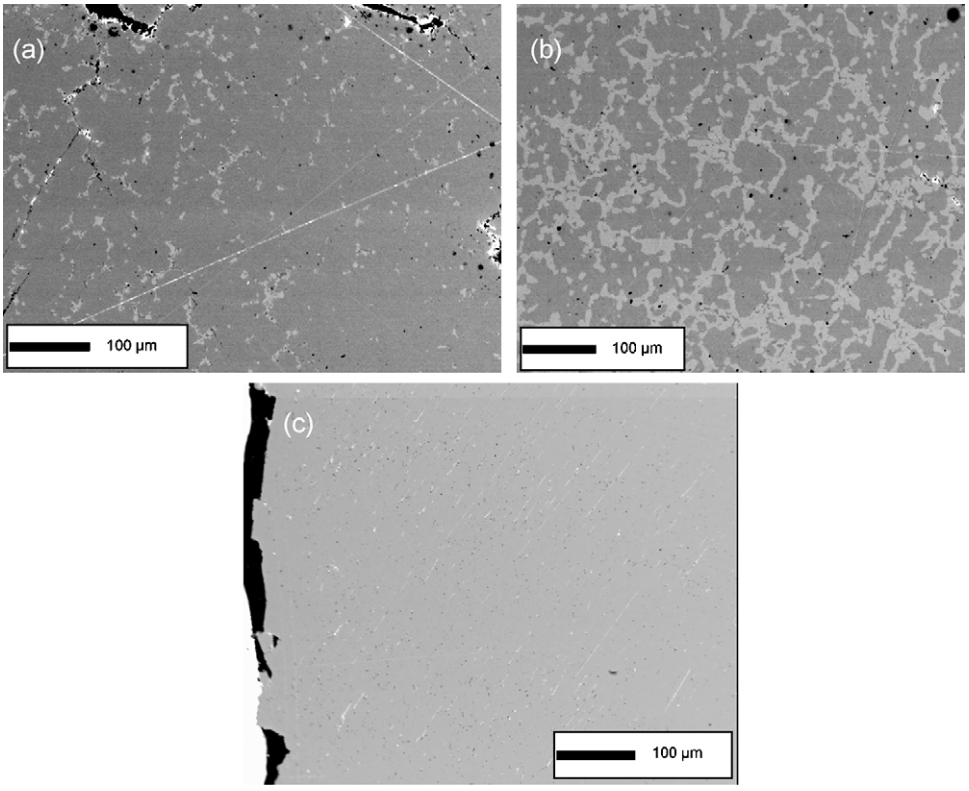

Fig. 4. BSE image of (a) sample 1, (b) sample 3 and (c) sample 1′.

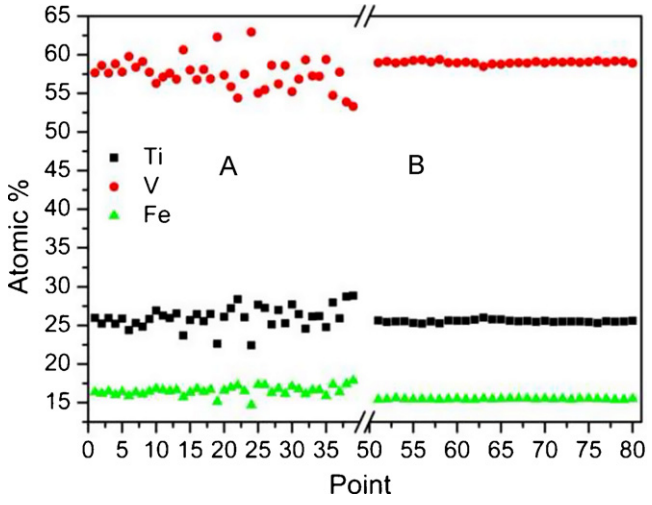

Fig. 5. Variation of the chemical composition of (A) the as-cast and (B) the annealed $Ti_{24.5}V_{59.3}Fe_{16.2}$ alloys (samples 1 and 1′) studied by EPMA.

precipitation of a small amount of *C*14 Laves phase during annealing.

The chemical composition of the inclusions present in the different compounds is similar (Table 1). The average composition is close to $Ti_{35.4}V_{32.3}Fe_{32.3}$ and belongs to the *C*14 domain proposed by Massicot et al. [22]. Small differences in the chemical composition of the matrix of the compounds are observed, particularly between compound 1 and compounds 2 and 3.

No significant difference in the chemical composition of the matrix of as-cast and annealed $Ti_{24.5}V_{59.3}Fe_{16.2}$ could be observed (Table 1). This shows that the annealing process does not affect the composition of the bcc matrix, only a small amount of *C*14 Laves phase appearing at the end of the annealing process, probably due to the decrease of the ternary solubilities at 1000 °C compared to higher temperature [22]. However more fluctuation in the internal chemical composition is observed for the as-cast sample due to the absence of a homogenization treatment (Fig. 5).

3.2. Hydrogenation properties

Let's first consider the end members of the series, namely the *C*14 Laves phase $Ti_{35.4}V_{32.3}Fe_{32.3}$ and the bcc compound $Ti_{24.5}V_{59.3}Fe_{16.2}$.

An exhaustive study of the hydrogenation properties of bcc Ti–V–Fe compounds has recently been reported by Massicot et al. [23]. The hydrogenation process of bcc alloys involves the formation of two hydrides [26,27]. For all hydrogen rich hydrides (capacity >0.9 H/fu), the PCI curves present a single equilibrium plateau for absorption and desorption with a significant hysteresis and a slight slope. In the case of annealed $Ti_{24.5}V_{59.3}Fe_{16.2}$, the compound could be fully hydrogenated at 25 °C during the first activation process. The PCI curves obtained in the present work (Fig. 6) are similar to that reported by Massicot et al. and Challet et al. [10,23]. This alloy can absorb up to 3.2 wt% hydrogen. However, because of the stability of the monohydride, hydrogen cannot be fully desorbed unless heating the material up to 500 °C.

The hydrogenation properties of the *C*14 Laves $Ti_{35}V_{30}Fe_{35}$ collected by Massicot are reported here [24]. The material is much more brittle than the bcc alloys and can be easily reduced to a fine powder. It could be fully hydrogenated at the end of the first activation. The trend in the PCI curves is very different from that described above for the bcc materials (Fig. 6). No equilibrium plateau could be observed. The interesting feature is the absence of hysteresis, which means that all the hydrogen stored inside the material can

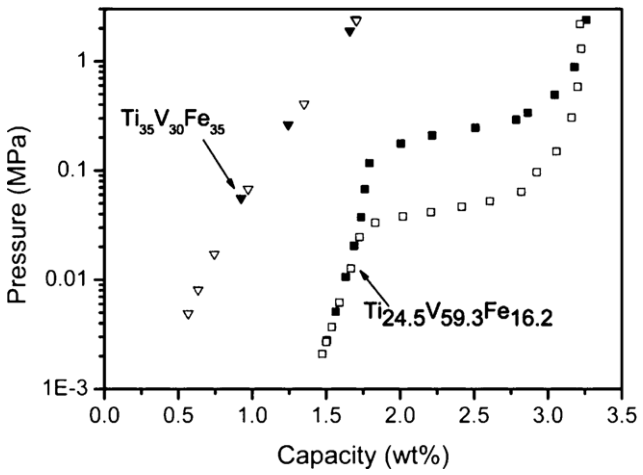

Fig. 6. PCI curves at 25 °C for $Ti_{24.5}V_{59.3}Fe_{16.2}$ (alloy 1) and $Ti_{35}V_{30}Fe_{35}$ (alloy 4). Absorption data correspond to plain symbols, desorption data to empty ones.

be released upon desorption. The maximum absorption capacity of the *C*14 laves phase is lower than that of the bcc compound $Ti_{24.5}V_{59.3}Fe_{16.2}$: the maximal absorption capacity is 3.2 wt% for $Ti_{24.5}V_{59.3}Fe_{16.2}$ and only 1.7 wt% for $Ti_{35}V_{30}Fe_{35}$. However, the reversible absorption capacities are not so different (~1.1 wt% for $Ti_{35}V_{30}Fe_{35}$ and ~1.8 wt% for $Ti_{24.5}V_{59.3}Fe_{16.2}$). These data agree with the hydrogenation properties reported by Miyamura et al. who

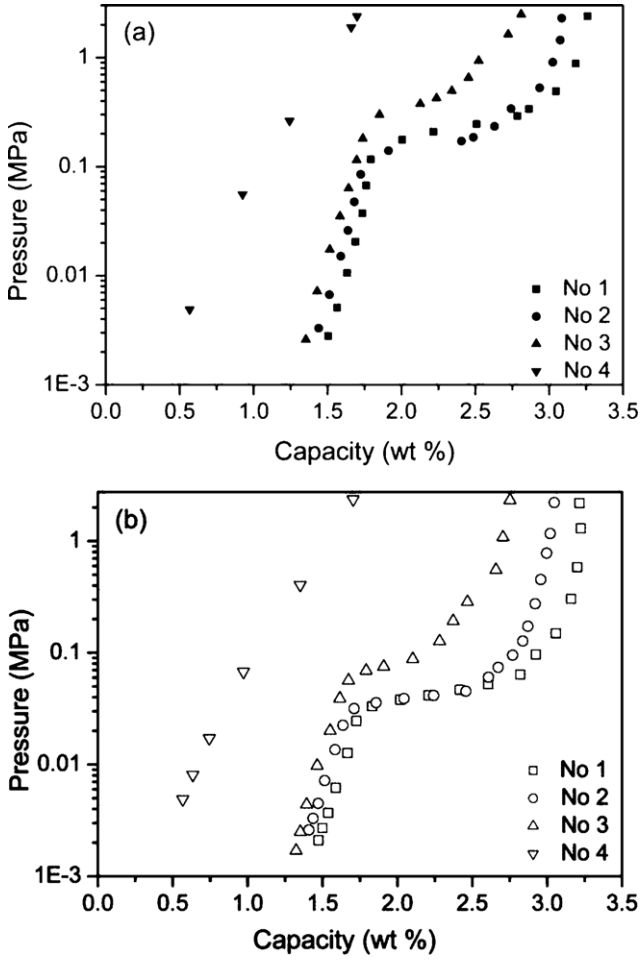

Fig. 7. (a) Absorption and (b) desorption PCI curves at 25 °C for compounds 1 (3.8 wt% *C*14), 2 (9.6 wt% *C*14), 3 (24.7 wt%) and 4 (100 wt% *C*14).

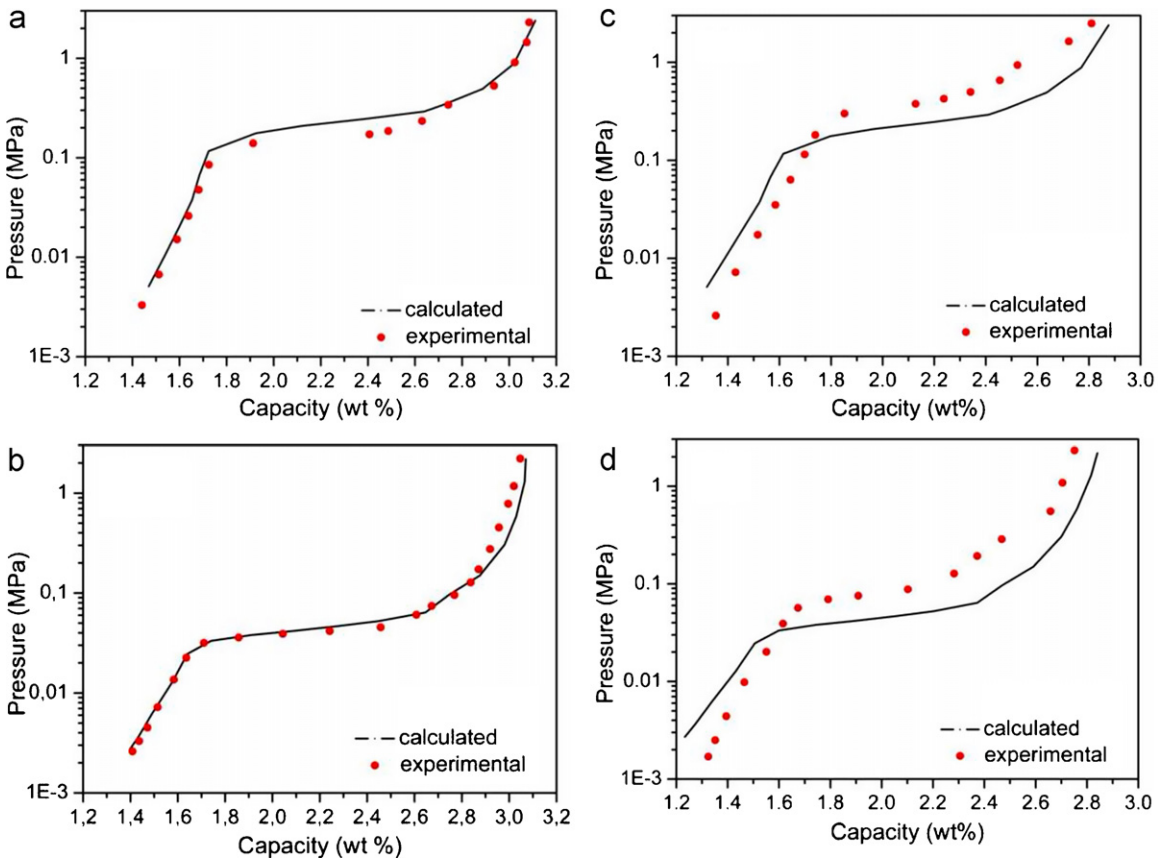

Fig. 8. Calculated and experimental PCI curves for compound 2 containing 9.6 wt% of *C*14 Laves phase ((a) absorption, (b) desorption) and for compound (3) containing 24.7 wt% of *C*14 Laves phase ((c) absorption and (d) desorption).

studied the *C*14 phases $Ti_{30}V_{10}Fe_{60}$, $Ti_{20}V_{20}Fe_{60}$ and $Ti_{37}V_{26}Fe_{37}$ [28].

The multiphase compounds 1, 2 and 3 could be easily fully activated during the first hydrogenation process. However hydrogenation experiments on different pure bcc compositions showed that the samples could not always be fully activated during the first hydrogenation: a thermal treatment at 500 °C under primary vacuum is often necessary for the sample to absorb the maximal hydrogen amount. The presence of a second phase in the bcc matrix can help hydrogen to penetrate more rapidly through the bulk because of the presence of grain boundaries. Besides, the second phase inclusions weaken the mechanical properties of the compound: single bcc phases are very strong and hard to break into pieces whereas compounds containing a second phase can be reduced to a coarse powder more easily.

The PCI curves were collected at 25 °C for all samples during absorption and desorption (Fig. 7a and b). The maximum absorption capacity and the length of the equilibrium plateau decrease with the content of second phase: the maximal absorption capacity is 3.2 wt% for $Ti_{24.5}V_{59.3}Fe_{16.2}$ and only 2.8 for $Ti_{27.45}V_{51.5}Fe_{21.05}$ (30% second phase). Compounds 1 and 2 have very similar PCI curves and the same plateau pressures (0.22 and 0.16 MPa, respectively). The plateau pressure of compound 3 is slightly higher (0.38 MPa): its value should be close to that of compounds 1 and 2. The explanation is probably the slight difference in the composition of the matrix: the matrix of compound 3 is slightly richer in Ti and Fe than that of compounds 1 and 2. This results in a higher equilibrium pressure.

In order to verify that the resulting PCI curves of the multiphase alloys are the sum of the proportional contributions of each phase, the calculated PCI curves are represented in Fig. 8. A difference in the plateau pressure is observed for compound 3: this can be attributed to a difference in the chemical composition of the matrix as mentioned above. A good agreement between calculated and experimental data is obtained for compound 2.

The annealing process can be a crucial economic factor for mass production. In order to evaluate the influence of the annealing on the hydrogenation properties of $Ti_{24.5}V_{59.3}Fe_{16.2}$, the PCI curves of an annealed and an as-cast sample are compared in Fig. 9. The absorption kinetics are slower in the case of the as-cast sample (90% of the maximal absorption capacity reached after 586 s). Both

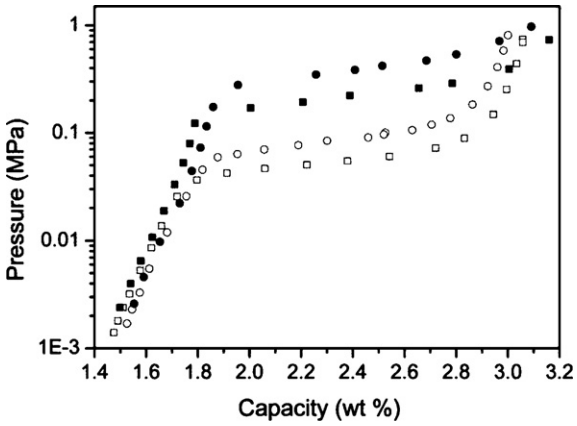

Fig. 9. PCI curves for as-cast (circles) and annealed (squares) $Ti_{24.5}V_{59.3}Fe_{16.2}$ (samples 1 and 1′). Absorption data correspond to plain symbols, desorption data to empty ones.

Table 2
Maximal capacity, reversible capacity, time to absorb 90% of the maximum capacity, equilibrium pressures for absorption and desorption measured at 25 °C under an initial hydrogen pressure of 2.5 MPa.

Sample No	Nominal composition	Maximal capacity (wt%) (±0.1)	Reversible capacity (wt%) (0.01–1 MPa) (±0.05)	t_{90} (s)	Equilibrium pressure for absorption (MPa) (±0.05)	Equilibrium pressure for desorption (MPa) (±0.05)
1	$Ti_{24.5}V_{59.3}Fe_{16.2}$	3.22	1.56	35	0.22	0.04
1′	$Ti_{24.5}V_{59.3}Fe_{16.2}$	3.18	1.43	586	0.42	0.10
2	$Ti_{25.6}V_{56.6}Fe_{17.8}$	3.08	1.48	32	0.16	0.04
3	$Ti_{27.45}V_{51.5}Fe_{21.05}$	2.81	1.11	46	0.38	0.08
4	$Ti_{35}V_{30}Fe_{35}$	1.70	0.84	24	No plateau	No plateau

curves exhibit similar trends. The main difference comes from the equilibrium pressures. Their values are higher for the as-cast sample: the plateau pressures are 0.42 and 0.10 MPa for the as-cast sample and 0.22 and 0.04 MPa for the annealed one (Table 2).

4. Conclusion

Several compounds with a bcc matrix of nominal composition $Ti_{24.5}V_{59.3}Fe_{16.2}$ containing 0, 10, 30% of *C*14 Laves phase were synthesized. The pure bcc phase $Ti_{24.5}V_{59.3}Fe_{16.2}$ was obtained only for the as-cast sample, a small amount of *C*14 laves being present in the annealed sample. The hydrogenation properties of the *C*14 Laves phase are very different from that of the bcc materials: the PCI curves do not have any equilibrium plateau and little hysteresis between absorption and desorption was observed. The maximum hydrogen absorption capacity of the *C*14 Laves phase is also lower than that of the bcc phase. Hydrogen can penetrate more easily the bulk of the multiphase alloys during the first activation because of the presence of grain boundaries but it does not change the absorption kinetics of the activated alloy. The hydrogen absorption capacity and the length of the equilibrium plateau decrease with the amount of secondary phase. Hence only a small amount of *C*14 Laves phase in the bcc is desirable for hydrogen storage application. The hydrogenation properties of the as-cast $Ti_{24.5}V_{59.3}Fe_{16.2}$ compound are quite similar to those of the annealed sample. The main differences are the absorption kinetics and the values of the hydrogenation pressures. As a result, the annealing step in the synthesis process does not seem that crucial.

Acknowledgements

The authors would like to thank Dr. E. Leroy for all EPMA analyzes and the ANR agency through the Pan-H program for funding.

References

[1] A.J. Maeland, J. Chem. Chem. 68 (1964) 2197.
[2] J.J. Reilly, R.H. Wiswall, J. Inorg. Chem. 9 (1970) 1678.
[3] S. Ono, K. Nomura, Y. Ikeda, J. Less-Common Met. 72 (1980) 159.
[4] A.J. Maeland, G.G. Libowitz, J.P. Lynch, J. Less-Common Met. 104 (1984) 361.
[5] S.W. Cho, C.S. Han, C.N. Park, E. Akiba, J. Alloys Compd. 288 (1999) 294.
[6] T. Tamura, A. Kamegawa, H. Takamura, M. Okada, Mater. Trans. JIM 42 (2001) 1862.
[7] H. Itoh, H. Arashima, K. Kubo, T. Kabutomori, J. Alloys Compd. 330–332 (2002) 287.
[8] M. Okada, T. Kuriiwa, A. Kamegawa, H. Takamura, Mater. Sci. Eng. A 329–331 (2002) 305.
[9] A. Kamegawa, K. Shirasaki, T. Tamura, T. Kuriiwa, H. Takamura, M. Okada, Mater. Trans. JIM 43 (2002) 470.
[10] S. Challet, M. Latroche, F. Heurtaux, J. Alloys Compd. 439 (2007) 294.
[11] J.-M. Joubert, M. Latroche, A. Percheron-Guégan, J. Bouet, J. Alloys Compd. 240 (1996) 219.
[12] M. Bououdina, D.-L. Sun, H. Enoki, E. Akiba, J. Alloys Compd. 288 (1999) 229.
[13] E. Akiba, H. Iba, Intermetallics 6 (1998) 461.
[14] D. Sun, J.M. Joubert, M. Latroche, A. Percheron-Guegan, J. Alloys Compd. 239 (1996) 193.
[15] M. Tsukahara, K. Takahashi, T. Mishima, A. Isomura, T. Sakai, J. Alloys Compd. 236 (1996) 151.
[16] H. Iba, E. Akiba, J. Alloys Compd. 231 (1995) 508.
[17] H. Iba, E. Akiba, J. Alloys Compd. 253–254 (1997) 21.
[18] B. Tsin Khua, I.I. Kornilov, Zh. Neorgan. Khimii 5 (1960) 434.
[19] B. Tsin Khua, I.I. Kornilov, Zh. Neorgan. Khimii 6 (1961) 694.
[20] V. Raghavan, in: I.I.O. Metals (Ed.), Phase Diagrams of Ternary Iron Alloys, ASM International, Calcutta, 1987, p. 73.
[21] L. Cornish, Watson, in: G. Effenberg, S. Ilyenko (Eds.), Ternary Alloy System, Subvolume D: Iron Systems, Part 5: Selected Systems from Fe–N–V to Fe–Ti–Zr, Springer, 2009, p. 668.
[22] B. Massicot, J.-M. Joubert, M. Latroche, Int. J. Mater. Res. 11 (2010) 1413.
[23] B. Massicot, M. Latroche, J.-M. Joubert, J. Alloys Compd. 509 (2011) 372.
[24] B. Massicot, PhD Thesis: Study of the Fe–Ti–V System and its Application for Hydrogen Storage, Paris XII, France, 2009, http://tel.archives-ouvertes.fr/index.php?halsid=iefog20oul60n714dsgpns4sl7&view_this_doc=tel-00442963&version=1.
[25] TOPAS3.0, in: DIFFRACPlus (Ed.), Bruker AXS, 2005.
[26] G.G. Libowitz, A.J. Maeland, Mater. Sci. Forum 31 (1988) 177.
[27] E. Akiba, M. Okada, MRS Bull. 27 (2002) 699.
[28] H. Miyamura, T. Sakai, N. Kuriyama, H. Tanaka, I. Uehara, H. Ishikawa, J. Alloys Compd. 253–254 (1997) 232.